Universal and Programmable Thinning and Thickening of Topologically-Active DNA Fluids

D. Michieletto,[1,2,*] P. Neill,[3] S. Weir,[4] D. Evans,[4] N Crist,[3] V. A. Martinez,[4] and R. M. Robertson-Anderson[3,†]

[1] *School of Physics and Astronomy, University of Edinburgh, Peter Guthrie Tait Road, Edinburgh, EH9 3FD, UK*
[2] *MRC Human Genetics Unit, Institute of Genetics and Cancer, University of Edinburgh, Edinburgh EH4 2XU, UK*
[3] *Department of Physics and Biophysics, University of San Diego, 5998 Alcala Park, San Diego, CA, 92110*
[4] *School of Physics and Astronomy, University of Edinburgh, Peter Guthrie Road, Edinburgh, EH9 3FD, UK*

Understanding and controlling the rheology of polymeric fluids that are out-of-equilibrium is a fundamental problem in biology and industry. For example, to package, repair, and replicate DNA, cells use enzymes to constantly manipulate DNA topology, length, and structure. Inspired by this impressive feat, we combine experiments with theory and simulations to show that complex fluids of entangled DNA display a rich range of non-equilibrium material properties when undergoing enzymatic reactions that alter their topology and size. We reveal that while enzymatically-active fluids of linear DNA display universal viscous thinning, circular DNA fluids - undergoing the same non-equilibrium process - display thickening with a rate and degree that can be tuned by the DNA and enzyme concentrations. Our results open the way for the topological functionalization of DNA-based materials via naturally occurring enzymes to create a new class of 'topologically-active' materials that can autonomously alter their rheological properties in a programmable manner.

The physics of non-equilibrium polymeric fluids is the basis for the design of next generation functional materials [1]. The majority of active matter systems considered thus far dissipate energy to drive the movement of their constituents [2–5]. On the contrary, activity-induced topological alterations remain largely unexplored [6–8]. In such "topologically-active" systems, energy may be dissipated to drive architectural or topological change in the constituents, which could be harnessed to drive a change in the bulk material properties.

Cellular DNA is a paradigmatic example of a topologically-active system in which a polymeric material, the genome, is kept out-of-equilibrium by proteins that continuously change its structure and topology to perform biological functions [9, 10]. One of the most widespread examples of topological alterations to genome architecture is restriction endonuclease reactions, such as in the CRISPR-Cas9 system [11]. Type II restriction endonucleases, specifically, are able to cleave the DNA backbone at specific restriction sites [12], and are now routinely employed in cloning and genome engineering. However, the rheological implications of these enzymes' action are often overlooked in spite of the fact that changes in solution viscoelasticity are commonplace in DNA extraction and purification assays.

At the same time, DNA has been extensively employed to study the physics of polymers in ring [13–17], supercoiled [18, 19] and linear topologies [20–23]. In equilibrium, solutions of concentrated ring polymers exhibit lower viscosity than their linear counterparts [17, 20, 24, 25], while blends of ring and linear polymers exhibit higher viscosity than pure linear chains [19, 25, 26].

* davide.michieletto@ed.ac.uk
† randerson@sandiego.edu

Inspired by the topological alterations of cellular DNA and the rich rheology that topologically-distinct polymers exhibit, here we couple time-resolved microrheology with non-equilibrium living polymer theory and Brownian Dynamics simulations to show that enzymatically-driven topological changes to DNA can induce programmable dynamics in complex polymeric fluids. Our results open up a novel class of active viscoelastic fluids whose constituents undergo topological alterations instead of translational motion. Our versatile yet generic framework can be harnessed for diverse applications from drug delivery to sensing devices. Additionally, they showcase the potential of protein-functionalised entangled DNA systems as a platform for the next generation of responsive materials.

Topology-dependent response to DNA digestion

We aim to understand the rheological implications of in situ digestion of DNA solutions by restriction enzymes (REs). We prepare entangled solutions comprised of two distinct types of DNA – large (48.5 kilobase-pairs (kbp)) linear λ-DNA and shorter (5.9 kbp) circular DNA. In standard cloning methods DNA digestion is performed at conditions that are not amenable to most material applications, including 37°C incubation, super-stoichiometric enzyme to DNA ratios, and DNA concentrations far below the polymer overlap concentration c^*. On the contrary, to harness enzymatically-driven topological changes for the modulation of functional materials, sustained room-temperature reaction rates (achieved with low stoichiometries) and viscosities that can be tuned by macromolecular topology (achieved at high DNA concentrations), are necessary. Further, bacteria need their endogenous endonucleases to routinely func-

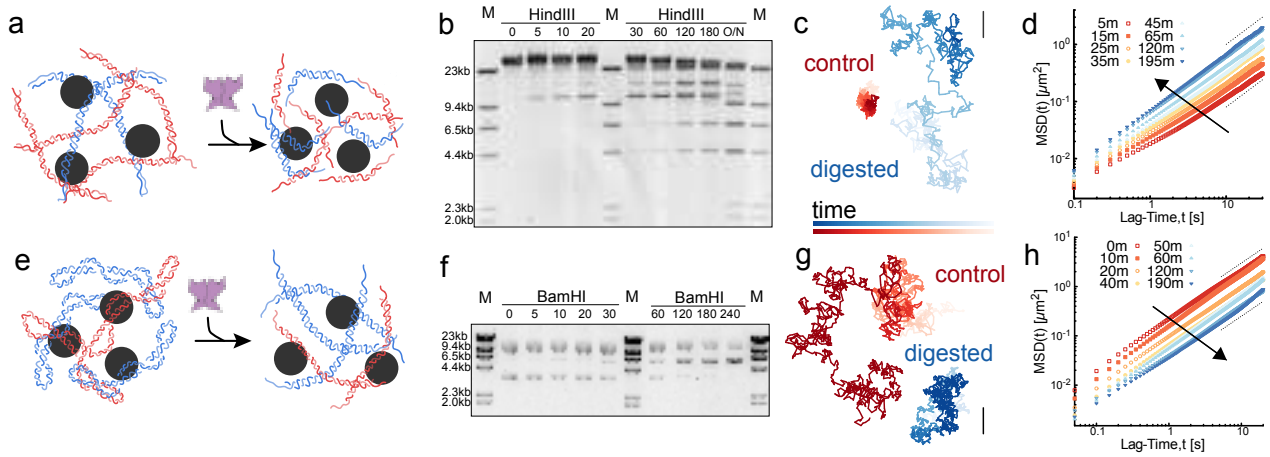

FIG. 1. **Topologically-active DNA fluids harness enzymatically-driven changes to DNA topology to self-alter their rheology**. **a,e** Entangled solutions of (a) 48.5 kbp linear λ-DNA and (e) 5.9 kbp circular PYES2 DNA (shown in red and blue) are spiked with microspheres (black) for particle-tracking microrheology. Addition of a restriction enzyme (RE, purple) triggers an irreversible architectural change to the DNA molecules. **b,f** Gel electrophoresis showing kinetic aliquots taken during "digestion" of entangled DNA by REs and showing progressive cutting of (b) λ-DNA by HindIII and (f) linearization of PYES2 by BamHI. In both gels, the marker (M) is λ-HindIII digest with fragments of well-defined length (shown on the left of the gels). In (f) bands corresponding to supercoiled and ring DNA are lower and higher than those for linear DNA of equal length, respectively. **c,g** Representative particle trajectories from microrheology in inactive (control, red) and digested (blue) solutions of (c) λ-DNA and (g) PYES2 plasmid DNA. Shading from dark to light indicates increasing time during tracking. Scale bar is 1 μm. **d,h** Mean squared displacements (MSD) at different times (shown in minutes in the legend) after the addition of (d) HindIII to λ-DNA and (h) BamHI to PYES2. The arrows point in the direction of increasing time after addition of the RE. The curves demonstrate a progressive thinning (d) and thickening (h) of the fluid over timescales of $\simeq 3-4$ hours. Dotted lines represent free diffusion $MSD \sim t$.

tion within crowded and entangled environments and at low stochiometric conditions *in vivo* [11]. This unconventional, yet functionally desirable and biologically relevant, regime is the focus of our work.

We discover that irreversible cleavage of entangled DNA yields a universal yet markedly topology-dependent response in the fluid viscosity. Specifically, while RE digestion of entangled linear DNA yields universal thinning that is enzyme-independent, the digestion of circular DNA triggers thickening that can be tuned by the concentration of both the DNA and RE (Fig. 1). To further demonstrate the rich active dynamics that can be achieved with enzymatically-driven DNA fluids, we show that we can design temporally-gated thinning following initial thickening using judiciously tuned RE types and concentrations.

Universal viscous thinning of entangled linear DNA under digestion

We first examine the behaviour of entangled λ-DNA undergoing digestion by different REs (Figs 1-2). Gel electrophoresis performed with kinetic aliquots taken at incremental times after the addition of the HindIII, an RE with 5 λ-DNA cleaving sites, shows that complete digestion takes $\gtrsim$ 3 hours (Fig. 1b). This result implies that the characteristic cutting time (per site) is $\tau_b = 1/\kappa \gtrsim 36$ minutes. To determine how digestion translates into rheology, we perform time-resolved microrheology by tracking diffusing microspheres for $\sim$2 minutes in 10-minute intervals over the course of 4 hours. As shown in Fig. 1c, representative particle trajectories with and without REs are dramatically different, with particles displaying a marked increase in displacement after full digestion. To quantify this effect we compute the 1D mean squared displacement (MSD) of the beads (Fig. 1d), which display an early subdiffusive regime, reflecting the viscoelasticity of the entangled DNA [28], crossing over to free diffusion after a few seconds, in agreement with the polymer relaxation time of $T_d \simeq 2$ s for entangled λ-DNA [28]. On the contrary, fully digested fluids display larger MSDs for any given lag time and no subdiffusive regime. The timescales over which the transition between these two regimes takes place aligns with the architectural re-arrangement seen in the electrophoresis (Fig. 1b).

The long-time behaviour of the MSDs suggest that the fluid is thinning over time, i.e. its viscosity is decreasing. To quantify this effect we compute the zero-shear viscosity using the Stokes-Einstein relation $\eta = k_B T/3\pi D a$, with $D = \lim_{t\to\infty} MSD(t)/2t$ and a the diameter of the tracer bead. We note that while our system is out-of-equilibrium, the digestion timescale (tens of minutes) is hundreds of times longer than the polymer relaxation ($T_d = 2$ s), such that the number of cleavages within one

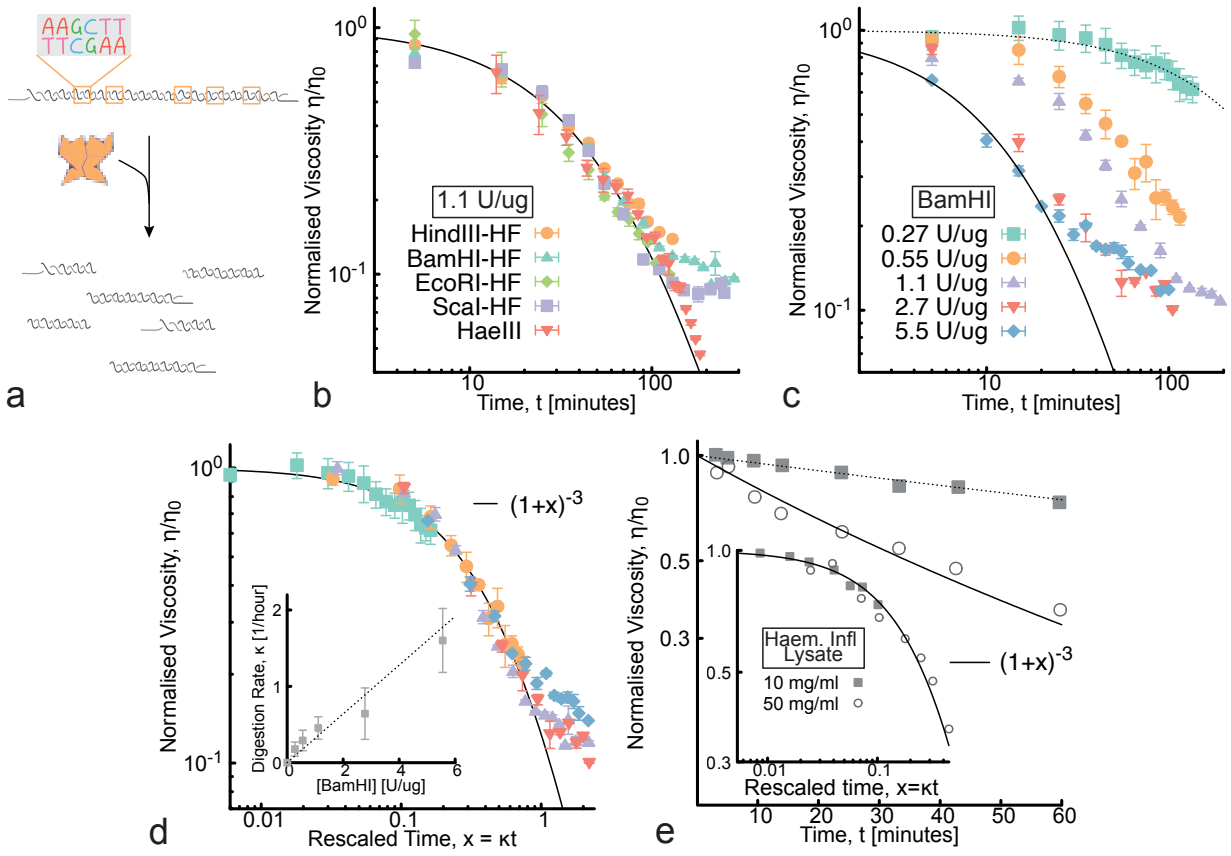

FIG. 2. **Universal thinning of entangled linear DNA via enzymatic digestion is described by non-equilibrium living polymer theory**. **a** Cartoon showing digestion of large linear DNA into smaller fragments via the action of a multi-cutter restriction enzyme. **b** Normalised viscosity η/η_0 for different multi-cutter restriction enzymes at fixed stoichiometry of 1.1 U/μg. The enzymes shown are (i) HindIII-HF (6-cutter, overhangs), (ii) BamHI-HF (5-cutter, overhangs), (iii) EcoRI-HF (5-cutter, overhangs), (iv) ScaI-HF (5-cutter, blunt ends) and (v) HaeIII (141-cutter, blunt ends). HF = "high fidelity", see SI for more information on REs. The solid curve is the predicted scaling of Eq. (1). ScaI-HF and BamHI-HF restriction sites leave large fragments of λ-DNA uncut, leading to deviation from the theory at large times. **c** Normalised viscosity η/η_0 as a function of time for different concentrations of BamHI-HF. By fitting these curves to $(1+\kappa t)^{-3}$ we find the digestion rate κ. **d** Data from (c) is collapsed onto a universal curve by rescaling time $t \to \kappa t$. Inset: Linear dependence of the cleavage rate $\kappa = \chi/T_d$ as a function of restriction enzyme concentration. **e** The first endonuclease discovered was HindII from Heamophilus Influenzae in 1970s [27]. The authors used a viscometric assay to prove that Heamophilus can digest the DNA of a P22 phage virus. The data shown in the seminal paper [27] is captured by our Eq. (1).

relaxation time is $\chi \equiv T_d/\tau_b \lesssim 10^{-3}$. Thus, we can consider our system to be in quasi-equilibrium with respect to the architectural degrees of freedom during each of our time-resolved measurements, allowing for unambiguous determination of diffusion coefficients and viscosity.

As shown in Fig. 2b, the viscosity of λ-DNA subject to HindIII digestion drops by over an order of magnitude over the course of a few hours. Quite strikingly, this phenomenon appears to be enzyme independent: the normalised viscosity η/η_0, where η_0 is the viscosity extrapolated to $t = 0$, for digestions by five different REs follows a universal master curve. These enzymes vary in the number of cleaving sites (5 to 141, see Fig. 2 caption) as well as in the lengths of the digested fragments (see SI for details). They also differ in whether they produce single-stranded overhangs or blunt ends at the cleaved site. Even with these variations, the system thins at the same rate at fixed RE:DNA stoichiometry.

We next examine the role of stoichiometry by considering BamHI ranging from ∼4-fold below to ∼5-fold above 1 U/μg. As expected, the thinning rate increases with increasing stoichiometry (Fig. 2c). By fitting the normalised viscosity curves to $\eta = \eta_0(1+\kappa t)^{-3}$ we obtain a direct measure of the digestion rate $\kappa = \chi/T_d = 1/\tau_b$ (see next section) which appears to be linear in enzyme concentration in agreement with Michaelis-Menten kinetics (Fig. 2d inset). Remarkably, upon rescaling time as $t \to x = \kappa t$, all curves collapse onto a single master curve that can be functionally described by a simple universal law $\eta/\eta_0 = (1+x)^{-3}$ (Fig. 2d).

DNA undergoing digestion is a non-equilibrium living polymer

To understand the master curve in Fig. 2 we propose a non-equilibrium generalisation of living polymer theory [29, 30]. The stress relaxation of a chain is related to the survival probability of its tube segments, $\mu(t)$, which for monodisperse and entangled polymer systems can be approximated as e^{-t/T_d} [31] where T_d is the longest relaxation (or "reptation") time $T_d(L_0) = L_0^2/(D_c\pi^2)$, with $D_c \sim D_0/L_0$ the curvilinear diffusion coefficient and D_0 a microscopic diffusion constant [31]. The stress relaxation can then be found as $G(t) = G_0\mu(t)$, with G_0 the instantaneous shear modulus and the zero-shear viscosity as $\eta_0 = \int_0^\infty G(t)dt \simeq G_0T_d$.

For entangled linear DNA undergoing digestion, irreversible cleavage must be taken into account in the chain relaxation process. Given the separation in timescales (recall $\chi \simeq 10^{-3}$) the fluid can be considered in quasi-equilibrium at any one time. The action of REs thus drives the system into a polydisperse state with mean length $\ell(t_a)$ that depends on the digestion time t_a. A mean field calculation yields [32] $\ell(t_a) = L_0/(n_c(t_a) + 1) = L_0/(\chi t_a/T_d + 1)$, where $n_c(t) + 1 = \chi t/T_d + 1 = t/\tau_b + 1$ is the average number of DNA fragments. The typical relaxation timescale at time t_a is that necessary for the relaxation of the average segment length with instantaneous curvilinear diffusion $D_c(t_a) = D_0/\ell(t_a)$, i.e., $\tau_r = \ell(t_a)^2/D_c(t_a) = (L_0^3/D_0)\,(\chi t_a/T_d + 1)^{-3}$. For small digestion times (compared with the typical breakage time $\tau_b = T_d/\chi$) the system behaves as if made by unbreakable chains with relaxation time $T_d \sim L_0^3/D_0$. In the opposite limit, one finds that $\tau_r \sim 1/(D_0\kappa^3t^3)$ up to times in which the reptation model is no longer valid. Accordingly, the zero shear viscosity is directly proportional to this relaxation timescale, i.e.

$$\eta(t_a) \simeq G_0\tau_r = \frac{\eta_0}{(\chi t_a/T_d + 1)^3}\,, \qquad (1)$$

with η_0 the zero shear viscosity before any digestion has happened.

Eq. (1) predicts that the thinning is independent of enzyme type as long as it displays a sufficient number (> 1) of restriction sites, as found in Fig. 2b. Eq. (1) also predicts that the key digestion rate is $\kappa = \chi/T_d$, expected to be proportional to enzyme concentration (Fig. 2c-d).

Curiously, the very first RE (HindII) was discovered by Smith and Welcox by measuring the viscosity of a solution made with phage virus (P22) DNA mixed with the lysate of a bacterium, Heamophilus Influenzae [27] using an Ostwald viscometer. Pleasingly, our theory perfectly captures the data they reported in their seminal paper [27] (Fig. 2e).

Viscous thickening triggered by digestion of entangled circular DNA

We next examine the rheological implications of digesting concentrated solutions of circular (plasmid) PYES2 DNA via a single-cutter RE, BamHI, that converts circular (supercoiled and ring) molecules into linear form (Fig. 1e,f and Fig. 3a). In striking contrast to the thinning seen for λ-DNA, our data displays clear viscous thickening (Figs. 1g-h). Particle trajectories become progressively more restricted over the course of hours, and the MSDs display a slowing down and the onset of a marginally subdiffusive regime at short times (Fig. 1h).

At fixed DNA concentration, the rate of thickening increases with increasing RE stoichiometry, indicating that thickening is directly linked to topological conversion into linear form (Fig. 3b,d). For the highest stoichiometry a plateau in viscosity is reached in < 2 hrs, mirroring complete digestion (Fig 3b), whereas at lower stoichiometries, the fluid continues to thicken over the course of the experiment. To understand this phenomenon, we recall that the radius of gyration, R_g, of linear DNA is larger than that for ring and supercoiled constructs of the same length ($R_{gL}/R_{gR} \simeq 1.6$ and $R_{g,L}/R_{g,SC} \simeq 2.1$ [19, 20]). This increase in R_g decreases the overlap concentration $c^* = (3L_0)/(4\pi R_g^3)$ as circles are converted to linear chains. The nature of entanglements is also topology dependent, with linear polymers exhibiting more persistent and dense entanglements compared to circular polymers, which in turn slows diffusion and increases viscoelasticity. Thus, it is rather intuitive that viscous thickening is triggered by linearisation of circular DNA and can be tuned by varying enzyme concentration.

Less intuitive is our results for digestions with fixed stoichiometry and varying DNA concentrations (Figs. 3c,e). While we find that the rate of digestion is independent of DNA concentration (Fig. 3c), we observe a pronounced impact of DNA concentration on the thickening behavior: the viscosity of the 6 mg/ml solution increases by nearly an order of magnitude during the digestion, whereas at 1.5 mg/ml thickening is nearly undetectable. To best understand these data we plot the normalized viscosity η/η_0 against c/c^*; note that while c is fixed, c^* is a function of R_g, and hence DNA topology, so it decreases during the digestion process. As shown in Fig 3f, our data collapses onto a master curve $\sim (c/c^*)^\gamma$ where $\gamma = 0.5$ at low c/c^*, crossing over to $\gamma = 1.75$ at large c/c^*. The crossover takes place at $c \simeq 6c^*$, which we previously showed to be at the onset of entanglement dynamics [20]. The exponents are the ones expected for semidilute ($c \simeq c^*$) and entangled ($c \gtrsim 6c^*$) DNA, respectively, and compatible with the behaviour of semidilute and entangled flexible polymers [31, 35].

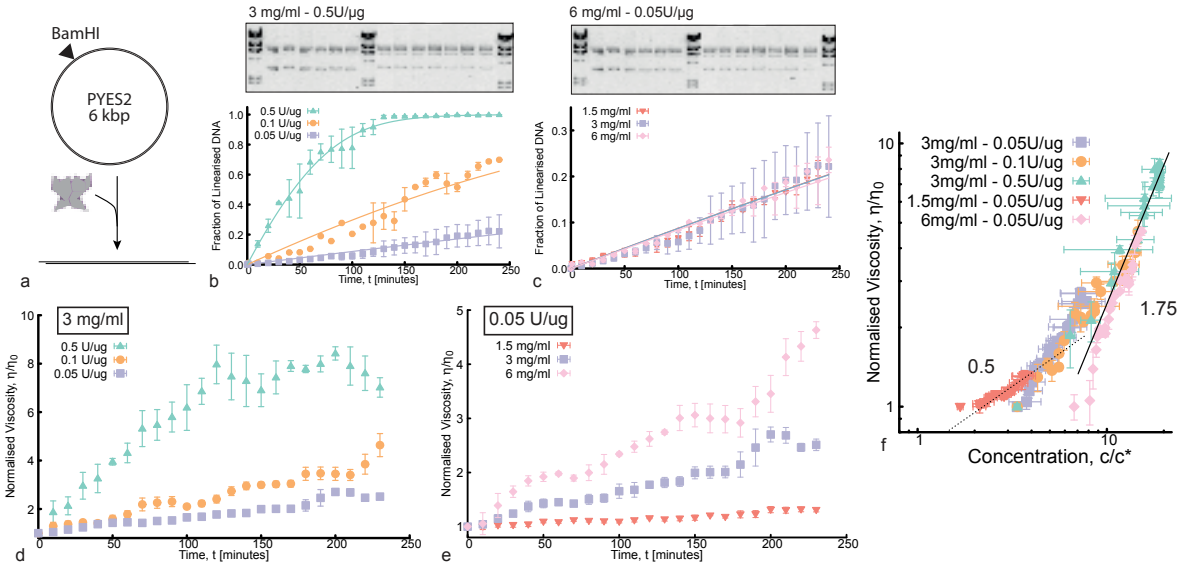

FIG. 3. **Viscous thickening of plasmid DNA during enzymatically-driven linearization is determined by intermolecular entanglements**. **a** Cartoon depicting digestion of a 6 kbp PYES2 plasmid DNA by a single-cutter RE (BamHI) that converts circular DNA to linear topology. **b,c** Topological conversion kinetics of PYES2 DNA versus digestion time, determined from quantification of gel electrophoresis bands (insets at the top) for varying (b) RE stoichiometries and (c) DNA concentrations. The data can be fitted with Michaelis-Menten (MM) kinetics (solid lines) with fixed Michaelis constant $k_M = 0.5$ μM, in line with values in the literature [33, 34]. **d,e** Normalised viscosity of the DNA fluids for fixed (d) DNA concentration and (e) RE stoichiometry. **f** Normalized viscosity η/η_0 plotted against DNA concentration c, normalized by the overlap concentration c^*. While DNA concentration c is fixed throughout the digestion, c^* decreases as circular DNA is enzymatically converted into linear topology. Dotted and solid lines show scalings of $\eta/\eta_0 \sim (c/c^*)^{0.5}$ and $\eta/\eta_0 \sim (c/c^*)^{1.75}$ predicted for Rouse-like [35] and entangled dynamics [31], respectively.

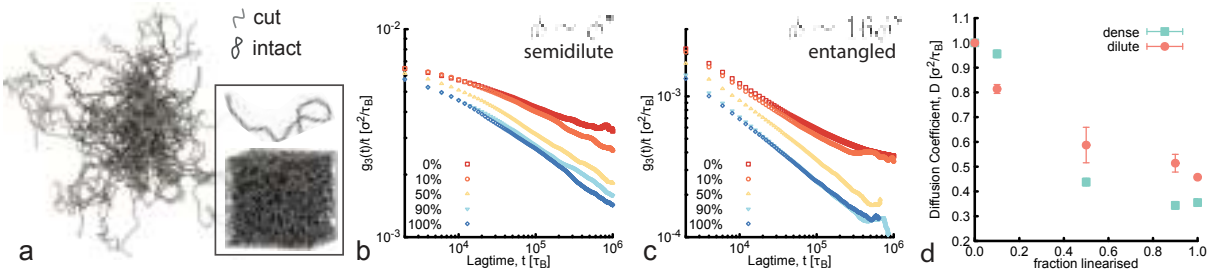

FIG. 4. **MD simulations reveal monotonic slowing down of DNA mobility under RE digestion**. **a** Simulation snapshot of entangled 6 kbp (M=800 beads) DNA in which 90% of molecules are linearized (cut, light grey) and 10% remain supercoiled (uncut, dark grey). The inset shows the same system in the simulation periodic box and a single uncut plasmid. **b,c** MSD of the centre of mass of the chains divided by lag-time, $g_3(t)/t$ and plotted against lag-time t for varying fractions of cut DNA (serving as a proxy for digestion time) for (b) dense (volume fraction $\phi = 4\%$ or $\phi/\phi^* \simeq 16$ with $\phi^* = 0.26\%$ [18]) and (c) semi-dilute (volume fraction $\phi = 0.24\% \simeq \phi^*$) regimes. MSDs and lag-time are in simulation units equivalent to $\sigma^2 = 6.25$ nm^2 and $\tau_B \simeq 0.03\mu$s (see SI). (d) Diffusion coefficients determined as $D = \lim_{t\to\infty} g_3(t)/6t$ showing a monotonic slowing down with increasing linear fraction.

Molecular dynamics simulations rationalise the monotonic thickening

At odds with recent works on blends of linear and ring polymers [19, 26], our results suggest that thickening is monotonic with the fraction of linear chains. To understand this effect, we perform Brownian Dynamics simulations of twistable chains [18, 36] modelling 6 kbp plasmids at volume fractions $\phi = 4\%$ and supercoiling degree $\sigma = 0.06$ [18] (see SI for details). We simulate the digestion by linearising a fraction $f = 0, 10, 50, 90$ and 100% of the chains to mimic different time points during digestion. We then let the system equilibrate (Fig. 4a) and measure the center-of-mass MSD of the DNA, $g_3(t)$. As shown in Fig. 4b, we find that the larger the fraction of cut plasmids, the monotonically slower the dynamics, in agreement with our data (Fig. 3). Additionally, the slowing down of the dynamics is stronger for higher

DNA concentration, as in the experiments (Fig. 3d). We note that the conformations of the plasmids are highly writhing due to the supercoiling (Fig. 4a) so we do not expect substantial threading by linear chains which may lead to non-monotonic thickening [26]. We expect that considering larger and relaxed circular (ring) DNA could trigger non-monotonic thickening, which will be the focus of future work.

Engineering gated thickening and thinning dynamics

Having demonstrated both thinning and thickening via irreversible DNA cleavage we next aim to achieve thickening followed by thinning and show that the magnitude and timing of the viscosity peak can be finely tuned using judiciously chosen cocktails of REs (Fig. 5a).

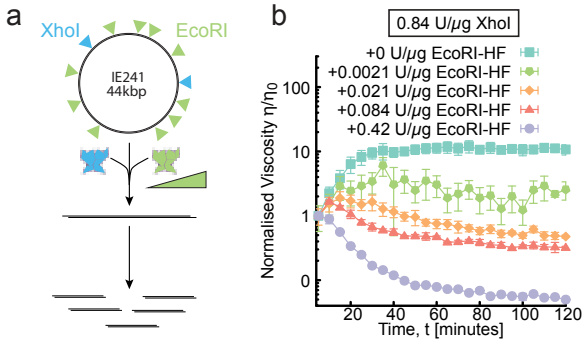

FIG. 5. **Programmable rheological gating of DNA complex fluids**. **a** We design 44 kbp plasmids (IE241) that can be cut twice or up to 10 times by different REs (XhoI and EcoRI, respectively). **b** Normalised viscosity versus digestion time for a 1.4 mg/ml solution of IE241 plasmids undergoing topological conversion by XhoI and EcoRI. Fluids exhibit initial thickening, due to XhoI-driven linearization, followed by thinning, due to fragmentation by EcoRI. The magnitude and timing of the viscosity peak, i.e., the onset of thinning, is tunable by the (i) type and (ii) stoichiometry of the multi-cutter RE.

To do so, we perform microrheology on 1.4 mg/ml solutions of 44 kbp circular DNA undergoing digestion by a combination of 2-cutter (XhoI) and 10-cutter (EcoRI) REs. As shown in Fig. 5b, the topologically-active solutions undergo a brief period of thickening, up to 1 hour, followed by slow thinning. The timepoint at which the peak in viscosity occurs, as well as its magnitude scales with the concentration of the 10-cutter. We expect the magnitude of the viscosity peak to be further controlled by the DNA concentration (as in Fig. 3) while the timing to remain independently tunable by multi-cutter concentration.

Conclusions

Here, we introduce a novel class of "topologically-active" complex fluids that are pushed out-of-equilibrium by microscopic changes in the topology of the constituents rather than translational motion. We create archetypal examples of these fluids using entangled DNA under the action of restriction enzymes, and characterize their properties by coupling time-resolved microrheology with non-equilibrium living polymer theory and molecular dynamics simulations. We demonstrate that these DNA fluids undergo time-dependent rheological changes that can be controlled by the size, topology and concentration of the DNA as well as the type and concentration of enzyme. Specifically, we show that fluids of large entangled linear DNA undergo universal viscous thinning during digestion by diverse multi-cutter enzymes, with dynamics that can be described by non-equilibrium living polymer theory. Conversely, we show that shorter circular DNA fluids exhibit viscous thickening during enzymatic conversion to linear topology, with a rate and degree that can be programmed by the concentrations of the DNA and enzyme. Finally, we demonstrate that these "topologically-active" fluids can exhibit even richer non-equilibrium rheology - undergoing initial thickening followed by time-gated thinning - that can be controlled by judicious combinations of enzymes and stoichiometries.

The adaptable and programmable self-driven systems that we present can be harnessed for diverse applications from autonomous tissue regeneration to infrastructure self-repair; and also shed light on the interplay between rheology and topology in key cellular processes such as replication and gene expression. More importantly, our results showcase the potential of harnessing non-trivial alterations to the structure and topology of DNA as a unique route to design, construct, and functionalize responsive and tunable non-equilibrium materials.

Acknowledgements DM acknowledges enlightening discussions with Rick Morgan (NEB) and Mark Szczelkun (Bristol) and thanks Aleksandre Japaridze for providing IE241 plasmids. DM is a Royal Society University Research Fellow and is supported by the European Research Council via a Starting Grant (Topologically Active Polymers, TAP, 947918). RMR-A acknowledges the US Air Force Office of Scientific Research (Grant no. AFOSR- FA9550-17-1-0249) for support.

[1] T. Sanchez, D. T. N. Chen, S. J. Decamp, M. Heymann, and Z. Dogic, Spontaneous motion in hierarchically assembled active matter, Nature **491**, 1 (2012), 1301.1122.

[2] M. C. Marchetti, J. F. Joanny, S. Ramaswamy, T. B. Liverpool, J. Prost, M. Rao, and R. A. Simha, Hydrodynamics of soft active matter, Rev. Mod. Phys. **85**, 1143

(2013).
[3] H. Mizuno, S. Mossa, and J. Barrat, Measuring Spatial Distribution of Local Elastic Modulus in Glasses, arXiv preprint arXiv:1301.4080 , 1 (2013), arXiv:1301.4080v1.
[4] J. Palacci, S. Sacanna, A. P. Steinberg, D. J. Pine, and P. M. Chaikin, Living Crystals of Light-Activated Colloidal Surfers, Science **339**, 936 (2013).
[5] N. J. Mlot, C. A. Tovey, and D. L. Hu, Fire ants self-assemble into waterproof rafts to survive floods, Proceedings of the National Academy of Sciences of the United States of America **108**, 7669 (2011).
[6] B. Kundukad and J. R. Van Der Maarel, Control of the flow properties of DNA by topoisomerase II and its targeting inhibitor, Biophysical Journal **99**, 1906 (2010).
[7] B. A. Krajina, A. Zhu, S. C. Heilshorn, and A. J. Spakowitz, Active DNA Olympic Hydrogels Driven by Topoisomerase Activity, Physical Review Letters **121**, 148001 (2018).
[8] L. Heinen and A. Walther, Programmable dynamic steady states in ATP-driven nonequilibrium DNA systems, Science Advances **5**, 32 (2019).
[9] C. R. Calladine, H. Drew, F. B. Luisi, A. A. Travers, and E. Bash, *Understanding DNA: the molecule and how it works*, Vol. 1 (Elsevier Academic Press, 1997) arXiv:1011.1669v3.
[10] A. Bates and A. Maxwell, *DNA topology* (Oxford University Press, 2005).
[11] M. Jinek, K. Chylinski, I. Fonfara, M. Hauer, J. A. Doudna, and E. Charpentier, A programmable dual-RNA-guided DNA endonuclease in adaptive bacterial immunity, Science **337**, 816 (2012).
[12] A. Pingoud, G. G. Wilson, and W. Wende, Type II restriction endonucleases - A historical perspective and more, Nucleic Acids Research **42**, 7489 (2014).
[13] D. M. Wulstein, K. E. Regan, J. Garamella, R. J. McGorty, and R. M. Robertson-Anderson, Topology-dependent anomalous dynamics of ring and linear DNA are sensitive to cytoskeleton crosslinking, Science Advances **5**, eaay5912 (2019).
[14] R. M. Robertson and D. E. Smith, Self-diffusion of entangled linear and circular DNA molecules: Dependence on length and concentration, Macromolecules **40**, 3373 (2007).
[15] Y. Zhou, K. W. Hsiao, K. E. Regan, D. Kong, G. B. McKenna, R. M. Robertson-Anderson, and C. M. Schroeder, Effect of molecular architecture on ring polymer dynamics in semidilute linear polymer solutions, Nature Communications **10**, 1 (2019).
[16] B. W. Soh, A. R. Klotz, R. M. Robertson-Anderson, and P. S. Doyle, Long-Lived Self-Entanglements in Ring Polymers, Physical Review Letters **123**, 048002 (2019).
[17] K. R. Peddireddy, M. Lee, C. M. Schroeder, and R. M. Robertson-Anderson, Viscoelastic properties of ring-linear DNA blends exhibit nonmonotonic dependence on blend composition, Physical Review Research **2**, 1 (2020), 2004.00133.
[18] J. Smrek, J. Garamella, R. Robertson-anderson, and D. Michieletto, Topological Tuning of DNA Mobility in Entangled Solutions of Supercoiled Plasmids, Science Advances , 1 (2021).
[19] K. R. Peddireddy, M. Lee, Y. Zhou, S. Adalbert, S. Anderson, C. M. Schroeder, and R. M. Robertson-Anderson, Unexpected entanglement dynamics in semidilute blends of supercoiled and ring DNA, Soft Matter **16**, 152 (2019).
[20] R. M. Robertson and D. E. Smith, Strong effects of molecular topology on diffusion of entangled DNA molecules., Proc. Natl. Acad. Sci. USA **104**, 4824 (2007).
[21] C. D. Chapman and R. M. Robertson-Anderson, Nonlinear microrheology reveals entanglement-driven molecular-level viscoelasticity of concentrated DNA, Phys. Rev. Lett. **113**, 1 (2014).
[22] T. T. Perkins, D. E. Smith, and S. Chu, Direct observation of tube-like motion of a single polymer chain, Science **264**, 819 (1994).
[23] M. Khan, K. Regan, and R. M. Robertson-Anderson, Optical tweezers microrheology maps the dynamics of strain-induced local inhomogeneities in entangled polymers, Phys. Rev. Lett. **123**, 038001 (2019).
[24] M. Kapnistos, M. Lang, D. Vlassopoulos, W. Pyckhout-Hintzen, D. Richter, D. Cho, T. Chang, and M. Rubinstein, Unexpected power-law stress relaxation of entangled ring polymers., Nature materials **7**, 997 (2008).
[25] C. Chapman, S. Shanbhag, D. E. Smith, and R. M. Robertson, Complex effects of molecular topology on diffusion in entangled biopolymer blends, Soft Matter **8**, 9177 (2012).
[26] D. Parisi, J. Ahn, T. Chang, D. Vlassopoulos, and M. Rubinstein, Stress Relaxation in Symmetric Ring-Linear Polymer Blends at Low Ring Fractions, Macromolecules **53**, 1685 (2020).
[27] H. O. Smith and K. W. Welcox, A Restriction enzyme from Hemophilus influenzae. I. Purification and general properties, Journal of Molecular Biology **51**, 379 (1970).
[28] X. Zhu, B. Kundukad, and J. R. Van Der Maarel, Viscoelasticity of entangled λ-phage DNA solutions, J. Chem. Phys. **129**, 1 (2008).
[29] D. Michieletto, Non-equilibrium living polymers, Entropy **22**, 1 (2020), 2009.05292.
[30] M. E. Cates, Reptation of Living Polymers: Dynamics of Entangled Polymers in the Presence of Reversible Chain-Scission Reactions, Macromolecules **20**, 2289 (1987).
[31] M. Doi and S. Edwards, *The theory of polymer dynamics* (Oxford University Press, 1988).
[32] This should be treated as a Poisson process but as we shall see the mean field approximation also yields good results.
[33] Q. Huang and E. Quiñones, A spectroscopic method to determine the activity of the restriction endonuclease EcoRV that involves a single reaction, Analytical Biochemistry **497**, 103 (2016).
[34] Z. Tong, B. Zhao, G. Zhao, H. Shang, and Y. Guan, 2'-O-methyl nucleotide modified DNA substrates influence the cleavage efficiencies of BamHI and BglII, Journal of biosciences **39**, 621 (2014).
[35] A. Dobrynin, R. Colby, and M. Rubinstein, Scaling theory of polyelectrolyte solutions, Macromolecules **28**, 1859 (1995).
[36] C. A. Brackley, A. N. Morozov, and D. Marenduzzo, Models for twistable elastic polymers in Brownian dynamics, and their implementation for LAMMPS., J. Chem. Phys. **140**, 135103 (2014).

Universal and Programmable Thinning and Thickening of Topologically-Active DNA Fluids: Supplementary Information

D. Michieletto,[1,2,*] P. Neill,[3] S. Weir,[4] D. Evans,[4] V. A. Martinez,[4] N. Crist,[3] and R. M. Robertson-Anderson[3,†]

[1] *School of Physics and Astronomy, University of Edinburgh, Peter Guthrie Tait Road, Edinburgh, EH9 3FD, UK*
[2] *MRC Human Genetics Unit, Institute of Genetics and Molecular Medicine, University of Edinburgh, Edinburgh EH4 2XU, UK*
[3] *Department of Physics and Biophysics, University of San Diego, 5998 Alcala Park, San Diego, CA, 92110*
[4] *School of Physics and Astronomy, University of Edinburgh, Peter Guthrie Road, Edinburgh, EH9 3FD, UK*

I. METHODS

1. DNA and restriction endonucleases

For the data shown in Figs 1 and 2 we use λ-DNA (48.5 kilobasepairs (kbp)), supplied from New England Biolabs at 0.5 mg/ml in TE (10 mM Tris-HCl, 1 mM EDTA, pH 8) buffer (N3011), which we concentrate to 1 mg/ml via ethanol precipitation. The day before a digestion experiment, a 100 μl DNA sample is incubated at 60°C for 5 minutes and quenched with 1 μl of a 100 μM solution of 12 bp single-stranded DNA oligos purchased from IDT (GGGCGGCGACCT and AGGTCGCCGCCC, ∼10:1 stochiometric ratio) to avoid hybridisation of λ-DNA due to complementary overhangs at the cos sites. For data shown in Figs 1 and 3, we use PYES2 DNA (5.9 kbp) prepared via replication of cloned plasmids in Escherichia coli, followed by extraction, purification, and vacuum concentration using previously described protocols [1, 2]. The resulting 13 mg/ml stock DNA solution, comprising 55% supercoiled circular topology and 45% nicked circular (ring) topology, is suspended in nanopure deionized (DI) water and stored at 4^oC. We quantify DNA concentration and topology via gel electrophoresis as decribed below (Fig S3). For data shown in Fig 5 we use a 44 kbp plasmid DNA (IE241, gift from Aleksandre Japaridze) prepared via replication of cloned plasmids in E coli followed by extraction. Stock solutions of IE241 are composed of supercoiled and nicked circular topologies (Fig S4). All restriction enzymes (RE) are purchased from New England Biolabs and stored at -20^oC. These RE include: HindIII-HF, BamHI-HF, EcoRI-HF, ScaI-HF, and HaeIII for λ-DNA digestions; BamHI-HF for PYES2 digestions; and XhoI and EcoRI-HF for IE241 digestions (Fig S4). For all RE, if available, we use the high-fidelity (HF) versions of these enzymes to reduce non-specific star activity.

2. Digestion reactions

RE digestion reactions are prepared by adding 1/10th of the final reaction volume of $10x$ reaction buffer supplied by the RE manufacturer (typically NEB CutSmart buffer) and 0.1% Tween-20 to the DNA solution (diluted to the desired concentration in nanopure DI water). Following mixing of the solutions by pipetting with a wide-bore pipet tip (to avoid shearing DNA) or putting on a roller, the RE is added and mixed and the solution is incubated at RT for the duration of the digestion. For λ-DNA, we perform digestions at DNA concentration c = 1.1 mg/ml DNA ($\sim 20x$ the overlap concentration $c^* \simeq 0.05$ mg/ml [3]) and stoichiometric ratios of enzyme units to DNA mass of 0.27 - 5.5 U/μg. For PYES2 DNA we use DNA concentrations c=1.5 - 6 mg/ml, corresponding to $\sim 2c^* - 8c^*$of the undigested solution of circular molecules and $\sim 9.5c^* - 38c^*$ for linear PYES2 DNA, and stoichiometric ratios of 0.01 - 0.5 U/μg. For the 44 kbp plasmid DNA (IE241) we use a DNA concentration of $c = 1.4$ mg/ml corresponding to $c/c^* \simeq 7$ and stoichiometries of 0.84 U/μg XhoI and 0-0.42 U/μg of EcoRI-HF. See Table S1 for details on the restriction enzymes used in this work.

RE	Site	Ends	λ-DNA	PYES2	IE241
HindIII	AAGCTT	overhang	6	-	2
BamHI	GGATCC	overhang	5	1	9
EcoRI	GAATTC	overhang	5	-	10
ScaI	AGTACT	blunt	5	-	2
HaeIII	GGCC	blunt	141	-	-
NotI	GCGGCCGC	overhang	0	-	-
XhoI	CTCGAG	overhang	1	-	2

TABLE S1. Table of the restriction enzymes used in this work. Columns are as follows: RE = name of restriction enzyme, Site = DNA basepair string in RE recognition site, Ends = type of cleaving the RE performs (leaving single-strand overhangs that are sticky or blunt ends that are not), λ-DNA = number of recognition sites on λ-DNA ; PYES2 = number of recognition sites on PYES2; IE241 = number of recognition sites on IE241. Dashes indicate that the combination was not tested.

* davide.michieletto@ed.ac.uk
† randerson@sandiego.edu

3. Gel electrophoresis

To characterize the rate at which REs digest DNA under the different conditions we use direct current agarose gel electrophoresis to separate the different topologies (linear, supercoiled, ring) and lengths of DNA. Specifically, we prepare a 40 μL digestion reaction as described above and incubate at RT for 4-12 hours. Every 5-10 minutes during the digestion we remove a 1 μL aliquot from the reaction and quench it with TE buffer and gel loading dye. We load 50 ng of DNA from each 'kinetic aliquot' onto a 1% agarose gel prepared with TAE buffer. We run the gel at 5 V/cm for 2.5 hours, allowing for separation of the DNA into distinct bands corresponding to supercoiled, ring, and linear DNA of varying lengths (Figs 1, 3, S3, S4). We use the standard λ-HindIII molecular marker (M) to calibrate the gel for determining topology, length and concentration of the different bands in our samples. We image gels using an E-Gel Imager (Invitrogen) and perform image intensity analysis to determine the relative concentrations of each band.

4. Microrheology

For microrheology experiments, we mix into the digestion reaction a trace amount of polystyrene microspheres (Polysciences), of diameter $a = 1$ μm, coated with Alexa-488-BSA to inhibit binding interactions with the DNA and visualize beads during measurements. We load the sample into a 100-μm thick sample chamber comprised of a microscope slide, 100 μm layer of double-sided tape, and a glass coverslip to accommodate a ~ 10 μL sample. The chambers are sealed with epoxy or petroleum jelly to avoid evaporation over the course of the several hour experiments. We perform experiments using an Olympus IX73 microscope with a $40x$ objective or a Nikon Eclipse Ts2 with $60x$ objective and Orca Flash 4.0 CMOS camera (Hamamatsu). We record time-series of diffusing beads starting ~ 5 mins after adding the RE to the sample (enough time for the epoxy to dry and to load the sample onto the microscope), taken to be t=0, and subsequent 10 minutes for the duration of the experiment. Time-series are collected for 100 - 120 seconds at 10 - 20 fps on a 1024x1024 field of view (imaging ~ 100 particles per frame), resulting in ~ 500 tracks per time-series.

Using TrackPy [4] along with custom-written particle-tracking code (Python and C++), we extract the trajectories of the diffusing beads and measure the time-averaged mean squared displacements (MSD) of the diffusing particles as a function of lag time Δt in the x and y directions. All MSDs shown (Figs 1, S2), and used to determine viscosities, are determined from the average of the MSDs in the x and y directions after removing potential drift. From the averaged MSDs, we compute the diffusion coefficient D via linear fits to the MSDs according to $MSD = 2D\Delta t$. From the diffusion coefficient D, we compute the viscosity η using the Stokes-Einstein equation $\eta = k_B T/(3\pi D a)$, with a the diameter of the diffusing particles. We note that for the highest DNA concentrations and longest digestion times modest viscoelasticity is observed at shorter times. In these cases we restrict our analysis to the terminal regime behavior in which the MSD scales linearly in time. Further, while this system is in a non-equilibrium state, estimates of the diffusion coefficients at each time point can be made using sufficiently small lag times (< 120 s) due to the slow rate over which noticeable changes in the dynamics occur and the separation of timescales related to polymer relaxation and digestion (i.e. $\chi = \mathrm{T}_d/\tau_b$).

5. Brownian Dynamics Simulations

DNA is modelled as a twistable elastic chain (as detailed in Ref. [5]) whereby the backbone is made of beads each decorated by three patches. The backbone beads interact via a purely repulsive Lennard-Jones potential as

$$U_{\mathrm{LJ}}(r) = \begin{cases} 4\epsilon \left[\left(\frac{\sigma_b}{r}\right)^{12} - \left(\frac{\sigma_b}{r}\right)^{6} + \frac{1}{4} \right] & r \le r_c \\ 0 & r > r_c \end{cases} , \quad (1)$$

where r denotes the separation between the bead centers. The cutoff distance $r_c = 2^{1/6}\sigma$ is chosen so that only the repulsive part of the Lennard-Jones is used. The energy scale is set by $\epsilon = \kappa_B T$ and the length scale by σ_b, both of which are set to unity in our simulations. Consistent with this, all quantities are reported in reduced LJ units. The size of each bead in real units should be considered as the thickness of DNA, i.e. $\sigma = 2.5$ nm or $= 2.5/0.34 \simeq 7.35$ bp per bead. The patches have no steric interactions.

Nearest-neighbour beads along the backbone are connected by finitely extensible nonlinear elastic (FENE) springs as

$$U_{\mathrm{FENE}}(r) = \begin{cases} -0.5kR_0^2 \ln\left(1 - (r/R_0)^2\right) & r \le R_0 \\ \infty & r > R_0 \end{cases} , \quad (2)$$

where $k = 40\epsilon/\sigma_b^2$ is the spring constant and $R_0 = 1.6\sigma_b$ is the maximum extension of the elastic FENE bond.

To model the persistence length of DNA (150 bp or 50 nm) we introduce an additional bending energy penalty between consecutive triplets of neighbouring beads along the backbone in order to control polymer stiffness:

$$U_{\mathrm{bend}}(\theta_b) = k_\theta \left(1 + \cos\theta_b\right) . \quad (3)$$

Here, θ_b is the angle formed between adjacent bonds, i.e. $\boldsymbol{t}_i \cdot \boldsymbol{t}_{i+1}/|\boldsymbol{t}_i||\boldsymbol{t}_{i+1}|$ with $\boldsymbol{t}_i$ the tangent at i, and $k_\theta = 20\kappa_B T$ is the bending constant. With this choice $l_p = 20\sigma_b \simeq 50$ nm is the persistence length.

To model the torsional stiffness, two dihedral CHARMM springs constrain the relative rotation of consecutive beads, ψ, at a user-defined value (ψ_0). The torsional angle ψ is determined as the angle between planes defined by the triplets bead-bead-patch running along

the DNA backbone. The potential is

$$U_{\text{torsion}}(\psi) = k_\psi \left[1 + \cos\left(n\psi - d\right)\right] \tag{4}$$

where $k_\psi = 50 k_B T$, $n = 1$ and $d = \psi_0$. The angle ψ_0 directly determines the thermodynamically preferred pitch of the twisted ribbon as $p = 2\pi/\psi_0$ and, in turn, this determines the preferred linking number as $Lk = M/p$, where M is the number of beads in the plasmid. In this model, we define the supercoiling as $\sigma \equiv Lk/M = 1/p$, which is set by initialising the patchy-polymer as a flat ribbon and by subsequently imposing the angle ψ_0 in order to achieve the desired σ (which may be zero, if $\psi_0 = 0$ or $p = \infty$).

Finally, to maintain consecutive beads parallel to the backbone, we constrain the angle between the triplets bead-bead-patch to $\pi/2$ so that the frames of reference formed by the triplets are aligned to each other. This potential is written as

$$U_{\text{align}} = k_a \left(1 + \cos\theta\right) \tag{5}$$

where θ is the tilt angle with $k_a = 200 k_B T$ (see also Ref. [6]).

The simulations are performed at fixed monomer density $\rho\sigma_b^3 = 0.08$ and $\rho\sigma_b^3 = 0.006$, equivalent to ∼39 mg/ml and 3 mg/ml of DNA ($\sigma_b = 2.5$ nm= 7.35 bp is the typical size of a bead). We evolve the equations of motion for the beads coupled to a heath bath which provides noise and friction. The equation of motion for each Cartesian component is thus given by

$$m_a \partial_{tt} r_a = -\nabla U_a - \gamma_a \partial_t r_a + \sqrt{2 k_B T \gamma_a}\,\eta_a(t)\,, \tag{6}$$

where m_a and γ_a are the mass and the friction coefficient of bead a, and η_a is its stochastic noise vector satisfying the fluctuation-dissipation theorem. U is the sum of the energy fields described above. The simulations are performed in LAMMPS [7] with $m = \gamma = k_B = T = 1$ and using a velocity-Verlet algorithm with integration time step $\Delta t = 0.002\,\tau_B$, where $\tau_B = \gamma\sigma^2/k_B T \simeq 0.03$ μs (using $\gamma = 3\pi\eta_{water}\sigma$ with $\eta_{water} = 1$ cP and $\sigma = 2.5$ nm) is the Brownian time.

To mimic different stages of DNA digestion by restriction enzymes with single restriction sites we remove a single bead from a different fraction f of rings together with the angles and dihedrals in which it is involved. Subsequently, we set the dihedral constant of all the dihedrals belonging to the fraction f of rings to $k_\psi = 0 k_B T$ mimicking fully relaxed linear segments of DNA.

[1] S. Laib, R. M. Robertson, and D. E. Smith, Preparation and Characterization of a Set of Linear DNA Molecules for Polymer Physics and Rheology Studies, Macromolecules **39**, 4115 (2006).

[2] R. M. Robertson, S. Laib, and D. E. Smith, Diffusion of isolated DNA molecules: dependence on length and topology., Proc. Natl. Acad. Sci. USA **103**, 7310 (2006).

[3] X. Zhu, B. Kundukad, and J. R. Van Der Maarel, Viscoelasticity of entangled λ-phage DNA solutions, J. Chem. Phys. **129**, 1 (2008).

[4] J. C. Crocker, M. T. Valentine, E. R. Weeks, T. Gisler, P. D. Kaplan, A. G. Yodh, and D. A. Weitz, Two-Point Microrheology of Inhomogeneous Soft Materials, Phys. Rev. Lett. **85**, 888 (2000).

[5] C. A. Brackley, A. N. Morozov, and D. Marenduzzo, Models for twistable elastic polymers in Brownian dynamics, and their implementation for LAMMPS., J. Chem. Phys. **140**, 135103 (2014).

[6] J. Smrek, J. Garamella, R. Robertson-anderson, and D. Michieletto, Topological Tuning of DNA Mobility in Entangled Solutions of Supercoiled Plasmids, Science Advances , 1 (2021).

[7] S. Plimpton, Fast Parallel Algorithms for Short-Range Molecular Dynamics, J. Comp. Phys. **117**, 1 (1995).

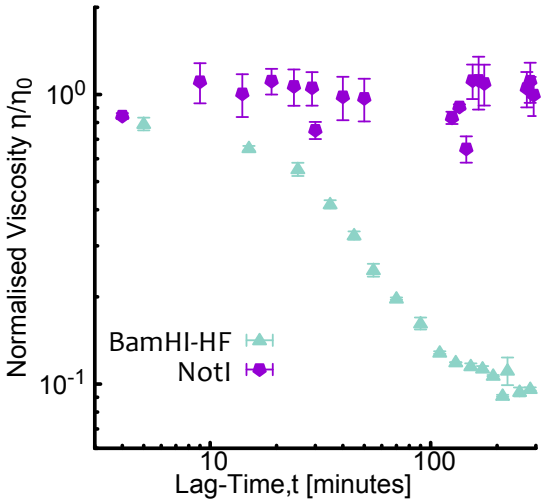

FIG. S1. Normalised viscosity of entangled λ-DNA undergoing digestion by BamHI-HF (5-cutter) compared to a RE that does not cut λ-DNA (NotI).

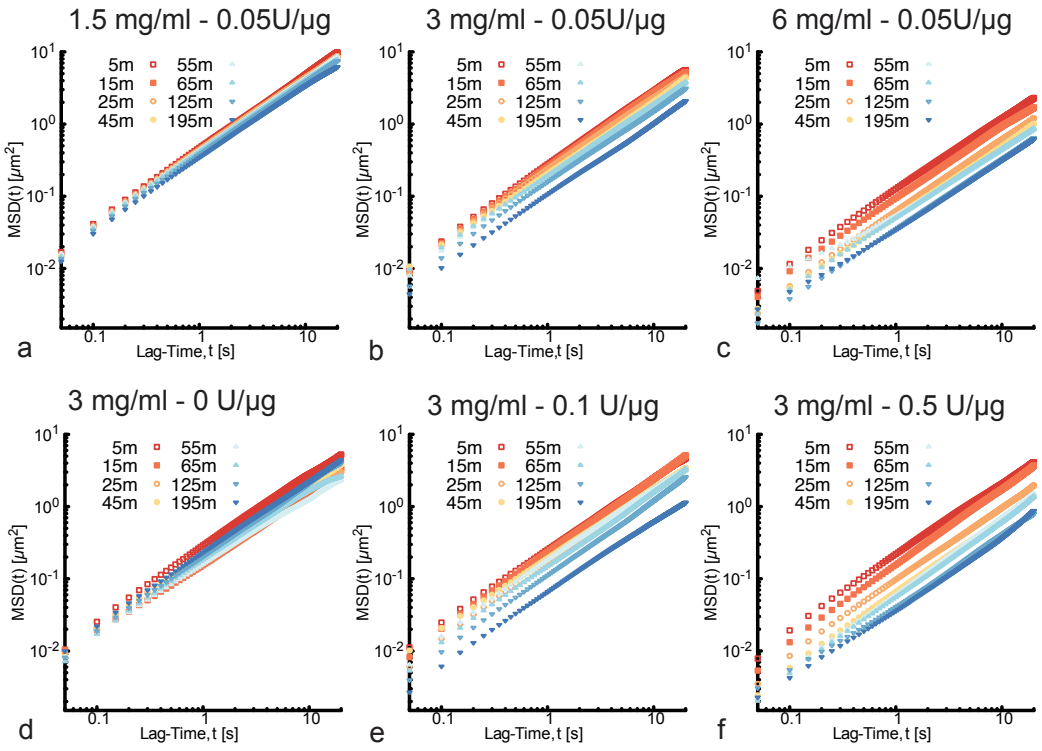

FIG. S2. *MSD*s for solutions of PYES2 DNA undergoing linearization by BamHI-HF at (top row) different DNA concentrations and fixed stoichiometry and (bottom row) different stoichiometry (including 0 U/µg) and fixed DNA concentration.

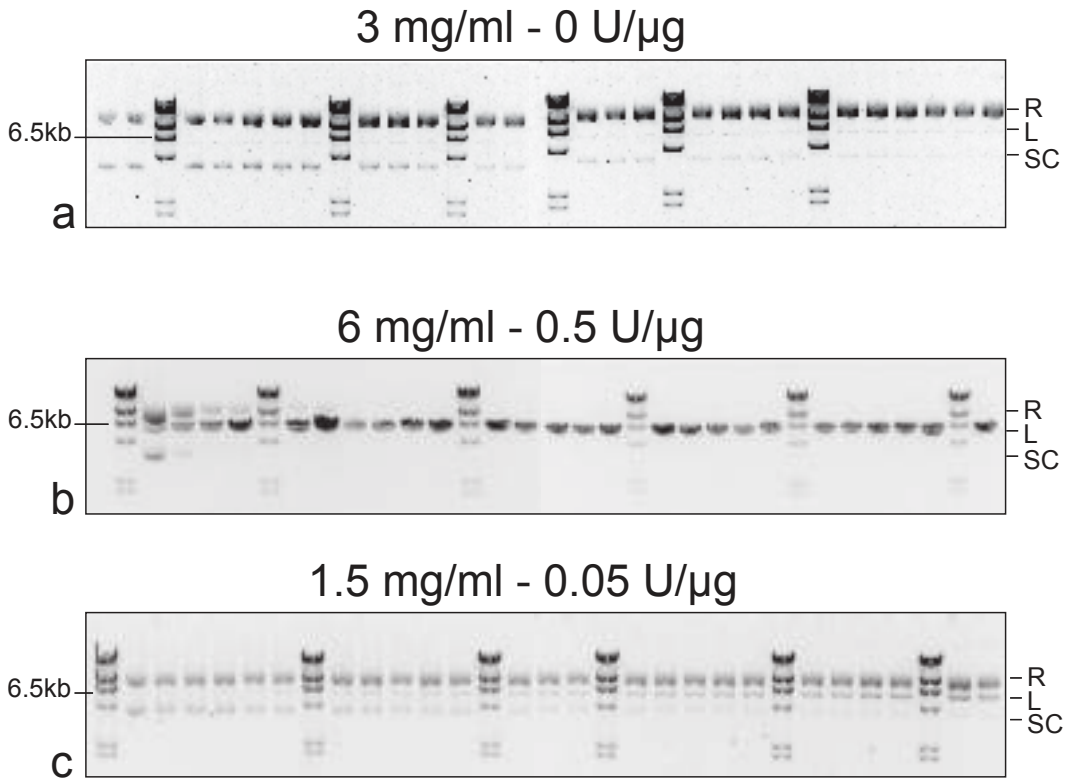

FIG. S3. Gel electrophoresis of PYES2 DNA undergoing digestion by BamHI-HF. In each gel the different lanes show the DNA topologies (L = linear, SC = supercoiled, R = ring) at varying time-points during the digestion starting at 0 min and proceeding in 10-minute intervals for 240 minutes. The DNA concentration and stoichiometry for (a),(b), and (c) are listed above the corresponding gel. Marker lanes (those with 6 bands) are the standard λ-HindIII ladder.

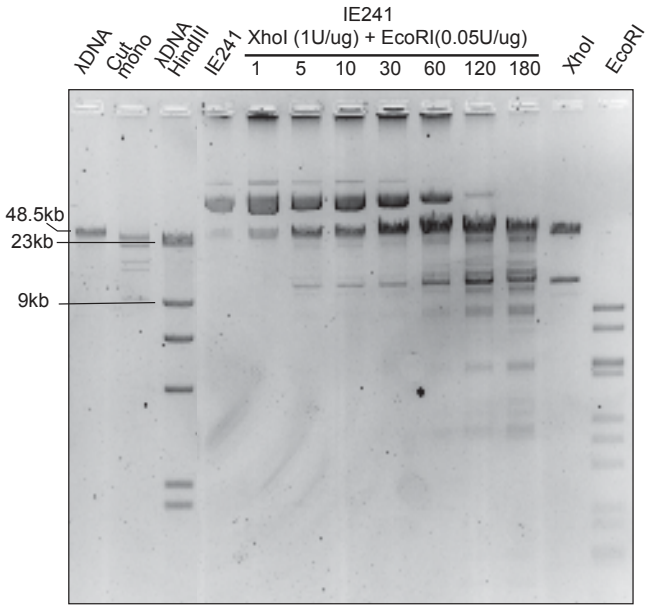

FIG. S4. Gel electrophoresis of IE241 plasmids undergoing digestion by a combination of XhoI (2-cutter) and EcoRI (10-cutter). The time during the digestion when each sample was collected is listed above the corresponding lane. The last two lanes show full digests by XhoI and EcoRI only.